Magna Scientia Advanced Research and Reviews

eISSN: 2582-9394

Cross Ref DOI: 10.30574/msarr

Journal homepage: https://magnascientiapub.com/journals/msarr/

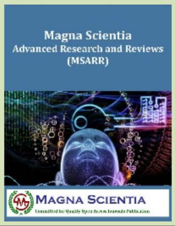

(REVIEW ARTICLE)

The Integration of PPP, Stand-Alone double differencing carrier phase relative positioning and MEMS-Based INS

Mustafa M. Amami *

Department of Civil Engineering, Benghazi University, Benghazi, Libya.

Magna Scientia Advanced Research and Reviews, 2026, 16(02), 018-034

Publication history: Received on 25 January 2026; revised on 06 March 2026; accepted on 06 March 2026

Article DOI: https://doi.org/10.30574/msarr.2026.16.2.0028

Abstract

The integration of Global Navigation Satellite Systems (GNSS) and Inertial Navigation Systems (INS) is widely recognized as an effective approach to overcome the individual limitations of each system, resulting in a navigation solution superior to either system operating independently. Similarly, the integration of kinematic Precise Point Positioning (PPP) with Stand-Alone Double Differencing Carrier Phase (SADDCP) enables the combination of the absolute positioning capability of PPP with the high precision and low satellite requirement of SADDCP, forming an Enhanced PPP (E-PPP) solution. Furthermore, SADDCP can be integrated with a Micro-Electro-Mechanical Systems (MEMS)-based INS to generate a Relative Navigation Solution (R-NS). In this integration, the high precision of SADDCP is utilized to smooth the noisy observations of the MEMS-INS, while the independence of the INS helps mitigate the impact of cycle slips affecting the carrier-phase measurements. In this study, the integration of PPP, SADDCP, and MEMS-INS is investigated to develop an innovative Enhanced PPP Navigation Solution (EPPP-NS), which combines the strengths of all three techniques while minimizing their individual weaknesses. The EPPP-NS is achieved through three levels of integration, namely: a loosely coupled integration between PPP and SADDCP to produce E-PPP, a loosely coupled integration between SADDCP and MEMS-INS to generate R-NS, and an uncoupled integration between E-PPP and R-NS to form the final EPPP-NS solution.

The performance of E-PPP, R-NS, and EPPP-NS was evaluated under various GNSS environments, including open-sky conditions, limited GNSS coverage, high-multipath scenarios, and complete GNSS outages. A pre-surveyed trajectory was used as a reference to ensure accurate performance assessment. Experimental results indicate that under open-sky conditions, the performance of E-PPP is comparable to that of raw PPP, with slight improvements observed in the height component. In partially obscured environments, E-PPP provides improved continuity and enhanced positioning quality compared to raw PPP. However, in heavily obscured or high-multipath environments, E-PPP performance deteriorates and is eventually lost when the number of connected satellites falls below two for planar positioning and below three for full 3D positioning. Regarding R-NS, as a relative positioning technique, it requires initialization from a known point, which represents its primary limitation. Nevertheless, experimental results demonstrate that R-NS can provide a smooth and acceptable navigation solution for short durations under open-sky conditions before experiencing gradual drift over time, without effective bounding, monitoring, or correction mechanisms. In partially and heavily obscured environments, R-NS maintains solution continuity and successfully mitigates the impact of cycle slips in SADDCP by utilizing smoothed INS observations. However, it still suffers from significant time-dependent drift.

The results confirm that EPPP-NS delivers the most stable and smoothed navigation solution compared to both E-PPP and R-NS across all tested scenarios. In open-sky environments, EPPP-NS achieves performance equivalent to E-PPP. Under partially obscured conditions, it demonstrates excellent robustness, where short interruptions in E-PPP are effectively bridged using the smoothed INS solution, ensuring continuous and stable navigation output. In high multipath areas, EPPP-NS has provided continues, precise, and smooth solution as long as the GNSS signals are available.

* Corresponding author: Mustafa M. Amami.

However, when GNSS signals are lost due to high multipath effect, the performance of EPPP-NS starts degrading until the connection with satellites returns back. During complete GNSS outages, EPPP-NS maintains acceptable performance as long as the influence of previously reliable SADDCP updates on the MEMS-INS, through the Kalman filter, remains effective. Beyond this period, the solution accuracy degrades over time, depending on the quality of the employed IMU sensor. Given this level of performance and robustness, EPPP-NS can be effectively applied in a wide range of engineering applications, including UAV surveying, mobile mapping systems, GIS data collection, and vehicle navigation in urban environments characterized by limited GNSS coverage and severe high-multipath effects.

Keywords: PPP; Double Differencing Carrier Phase Delta Positioning; IMU; GNSS/ MEMS-INS integration; Kalman filter

1. Introduction

Global Navigation Satellite Systems (GNSS) determine position and velocity through satellite-based passive ranging measurements [1]. Designed to provide continuous, global, and all-weather coverage, GNSS delivers accurate positioning and timing information worldwide [2]. Among GNSS positioning techniques, Precise Point Positioning (PPP) offers a globally consistent absolute solution without reliance on local reference stations [3]. PPP employs precise satellite orbit and clock corrections, typically provided by the International GNSS Service (IGS), in conjunction with rigorous atmospheric and relativistic modeling [4]. Under favorable conditions, PPP achieves centimeter-level accuracy in both static and kinematic modes; however, it generally requires longer convergence times compared with differential GNSS (DGNSS) techniques [5]. In contrast, positioning based solely on pseudo-range code observables provides absolute coordinates with typical three-dimensional accuracies at the meter level [6]. The error sources affecting GNSS techniques, including PPP and SADDCP, can be categorized into: (1) satellite-related errors (orbit and clock), (2) signal propagation errors (ionospheric delay, tropospheric delay, and multipath), and (3) receiver-related errors (receiver clock instability, measurement noise, and antenna phase center variations) [7]. Owing to its global applicability and independence from reference infrastructure, PPP has been widely adopted in numerous engineering applications, including vehicle navigation [8], drone operations [9], ortho-mosaic and digital elevation model generation [10], geodetic control, deformation monitoring, mobile mapping systems [11], GIS data acquisition, precision agriculture, disaster response, emergency management, and tourism [12].

Carrier-phase observations can be measured with a precision of approximately 0.01 cycles, corresponding to millimeter-level ranging accuracy. However, only the fractional phase and the accumulated integer number of wavelengths can be tracked as long as continuous satellite–receiver lock is maintained [13]. The unknown initial integer number of wavelengths, known as the integer ambiguity, prevents absolute stand-alone positioning from a single epoch using carrier-phase observations alone. To address this limitation, single- or multi-frequency differencing carrier-phase GNSS techniques are employed to provide precise relative positioning, which can subsequently be transformed into absolute positioning using at least one known reference point [14]. Through differencing, several GNSS error components are eliminated, while others are significantly reduced depending on their spatial and temporal correlation across the baseline. Differencing strategies include single, double, and triple differences [15]. A single difference may be formed between two receivers observing the same satellite at one epoch, or between one receiver observing one satellite at two epochs. A double difference is generated by differencing two single differences, while triple differences involve combinations across two receivers, two satellites, and two epochs [16].

Stand-Alone Double Differencing Carrier Phase (SADDCP) is a precise velocity estimation technique based on single-frequency GNSS observables. By integrating velocity estimates over time, accurate relative positioning can be achieved. SADDCP employs double differencing across two epochs and two satellites for a single receiver, effectively eliminating ambiguity and receiver clock errors, while significantly reducing satellite clock, orbit, ionospheric, and tropospheric errors due to high short-term correlation. Multipath effects remain partially correlated and may be moderately reduced, whereas receiver noise increases and accumulates over time [17].

An Inertial Navigation System (INS) consists of an Inertial Measurement Unit (IMU) integrated with a computational processing unit. The IMU comprises accelerometers and gyroscopes that continuously measure linear acceleration and angular velocity to estimate changes in position, velocity, and orientation [18]. INS performance depends primarily on initialization accuracy, sensor stability and reliability, and the applied error modeling and compensation algorithms. As a fully self-contained and passive navigation system, INS operates independently of external signals and is robust under all weather conditions. Consequently, INS has become indispensable in applications such as aircraft navigation, maritime and submarine operations, tactical and strategic missile systems, and spacecraft navigation [2]. Despite its advantages, INS cannot independently provide absolute positioning and requires accurate initial position and attitude information. Furthermore, INS is affected by various error sources, including accelerometer bias, gyro drift, initial misalignment, azimuth misalignment, and leveling errors. Because INS navigation is fundamentally based on integration of measured accelerations and angular rates, even small sensor biases accumulate over time, leading to significant drift. Therefore, INS must be integrated with an absolute positioning system to periodically correct accumulated errors, with the required update rate depending on IMU quality [13]. Micro-Electro-Mechanical Systems (MEMS)-based IMUs offer low cost, compact size, and lightweight characteristics, enabling broader deployment in applications such as human and animal motion capture [14]. MEMS gyroscopes exhibit advantages including low power consumption, rapid start-up time, absence of mechanical bearings or lubricants, and high mechanical robustness. However, MEMS-based IMUs are highly sensitive to temperature variations, require careful sampling of analog outputs, and exhibit relatively high gyro drift rates (20–30°/hour), limiting their suitability for high-precision navigation applications [18].

The integration of GNSS and INS effectively compensates for the weaknesses of each system, producing a navigation solution superior to either system operating independently. INS errors grow with time, whereas GNSS positioning errors are generally time-independent. INS provides high-rate motion and attitude information, while GNSS outputs are typically lower-rate but absolute. INS is fully autonomous, whereas GNSS depends on satellite visibility. Additionally, INS offers high-rate and accurate attitude determination, while GNSS-based attitude estimation is limited. Conversely, GNSS provides self-initialization capability, which INS lacks. In integrated systems, INS supports GNSS during signal blockages, reduces reacquisition time, and mitigates sensitivity to vehicle dynamics, while GNSS constrains INS drift and provides absolute position and attitude updates [14].

In [18], the integration of low-cost GNSS and MEMS-based INS sensors was comprehensively evaluated. The study demonstrated that low-quality stand-alone GNSS positioning, particularly in urban environments and at low-speeds, degrades IMU gyro performance, resulting in unstable and degraded navigation solutions. Furthermore, MEMS-based INS contributed limited improvement to GNSS positioning when satellite signals were available, and the integrated solution degraded rapidly during GNSS outages, contradicting the primary objectives of GNSS/INS integration. In [16], a loosely coupled integration of SADDCP with GNSS code positioning using a Kalman filter was investigated. The high-precision relative positioning from SADDCP was used to smooth low-accuracy absolute code positioning, yielding enhanced stand-alone single-frequency GNSS positioning. Experimental evaluation demonstrated improved absolute accuracy and continuity. The precision and multipath resistance of SADDCP enhanced degraded code solutions, while the absolute and continuous nature of code positioning mitigated SADDCP limitations, including its relative nature, cumulative error growth, and susceptibility to cycle slips. However, the integration required at least one accurately known reference point along the trajectory, typically obtained from a static code solution.

In [14], SADDCP was integrated with MEMS-based INS and evaluated under open-sky, limited-coverage, and indoor environments. Results indicated that a precise and low-cost relative navigation solution could be achieved under open-sky conditions with minimal multipath. However, solution quality degraded over time at rates of approximately 1.5–2 mm/s, depending on SADDCP quality. Increasing GNSS data rates (≥10 Hz) significantly improved performance by limiting IMU error growth. Under limited satellite visibility and high multipath conditions, SADDCP suffered from cycle slips, reducing overall solution quality. Although high-rate integration mitigated short-term cycle-slip effects, the solution remained cumulative and degraded over time. During complete GNSS outages lasting several minutes, positioning errors reached meter-level magnitudes within short durations [6].

In [13], a multi-level integration of GNSS code positioning, SADDCP, and MEMS-based INS was proposed to develop an Enhanced Absolute Navigation Solution (EA-NS). The framework comprised: (1) loosely coupled integration between code positioning and SADDCP to generate Enhanced Code Positioning (E-CP), (2) loosely coupled integration between SADDCP and MEMS-based INS to produce a Relative Navigation Solution (R-NS), and (3) uncoupled integration between E-CP and R-NS to obtain EA-NS. Experimental results demonstrated that EA-NS provided the most stable and smoothed navigation solution across diverse GNSS environments. Under open-sky conditions, EA-NS performance matched E-CP. Under weak-signal conditions, such as under tree canopy, EA-NS effectively mitigated cycle slips and degraded code performance. In high-multipath areas with intermittent satellite availability, EA-NS maintained continuity by bridging SADDCP interruptions using smoothed INS outputs. During complete GNSS outages, acceptable performance was maintained temporarily through prior SADDCP/INS Kalman filter updates, after which performance degraded depending on IMU quality. EA-NS was shown to be suitable for UAV surveying, mobile mapping, GIS data collection, and urban navigation in restricted-sky environments.

In [17], a loosely coupled integration of SADDCP relative positioning with raw kinematic PPP using forward and reverse Kalman filtering was proposed to enhance solution continuity, yielding Enhanced PPP (E-PPP). Precise three-dimensional relative positioning from SADDCP, available with at least three healthy satellites, was used to bridge PPP outages occurring during satellite shortages (<5 satellites) or ambiguity reconvergence. When only two satellites were available, planar positioning was maintained. Experimental validation over pre-surveyed trajectories demonstrated that, in open-sky conditions, raw PPP achieved 3–5 cm accuracy with full continuity, while E-PPP showed comparable or slightly improved performance, particularly in height. In partially obstructed environments, E-PPP improved raw PPP accuracy by approximately 0.7 m, 0.9 m, and 1.15 m in the east, north, and height components, respectively, while preserving full continuity. In heavily obstructed areas, raw PPP covered only 21% of the trajectory, whereas E-PPP achieved 65% (2D) and 89% (3D) continuity with substantially improved accuracy.

These findings confirm that SADDCP/PPP integration significantly enhances positioning continuity and robustness of raw PPP in challenging environments. Nevertheless, further research is required to integrate kinematic PPP/SADDCP with MEMS-based INS to mitigate prolonged outages and cumulative drift in severely obstructed conditions, which is the objective and focus of this study. Future research will extend this framework toward integration with vision-based navigation techniques for optical robots [19], [20] and UAV-based surveying applications, with the aim of improving exterior orientation parameters and reducing computational demands in automated image-matching workflows. Additional related work conducted at Benghazi University on integration strategies, drone-based surveying, and vision-assisted navigation can be found in [21–24].

Aim and objectives

In this paper, the integration of Precise Point Positioning (PPP), Stand-Alone Double-Differenced Carrier Phase (SADDCP), and a MEMS-based Inertial Navigation System (INS) is investigated to assess the feasibility of combining the strengths of these techniques while mitigating their individual limitations. First, the integration between PPP and SADDCP is presented, with all mathematical models adopted from [7]. Next, the integration between SADDCP and the MEMS-based INS is mathematically formulated, where the corresponding models and equations are derived from [6]. Finally, the outputs of the two previous integration stages are combined to produce the proposed Enhanced PPP Navigation System (EPPP-NS). The performance of the proposed system is evaluated along a precisely pre-surveyed trajectory under various GNSS conditions, including open-sky, limited satellite availability, high-multipath environments, and completely GNSS-denied areas. For data collection, a Leica GS10 triple-frequency GNSS receiver, a NovAtel tactical-grade IMU (HG1700 AG58), and an industrial-grade IMU (Microstrain 3DM-GX2) were used. The tightly coupled integration of the GS10 receiver and the NovAtel IMU is employed to generate the reference trajectory for performance evaluation. The reference solution is obtained using NovAtel Waypoint software, where GNSS/INS integration is performed in tightly coupled mode, and the GNSS–IMU lever-arm parameters are treated as unknowns and estimated as part of the navigation solution. The raw GNSS observations are processed using GrafNav software to obtain a kinematic PPP solution along with its associated standard deviation values. The three integration stages used in this paper are implemented using MATLAB algorithms developed by the author, based on the mathematical models presented in the following sections.

2. Methodology

2.1. Loosely Coupled Integration of SADDCP and PPP (E-PPP)

The loosely coupled integration between SADDCP and PPP is implemented using a self-developed MATLAB algorithm. The objective of this integration is to exploit the high relative precision and reduced satellite requirement of SADDCP to smooth and enhance the raw kinematic PPP solution under partially and heavily obscured sky conditions. At the same time, the absolute positioning capability of PPP is utilized to overcome the relative nature of SADDCP, resulting in the Enhanced PPP (E-PPP) solution. In this approach, the estimated position and velocity obtained independently from SADDCP and raw PPP are compared, and their differences are introduced into a Kalman filter as measurement updates. The redundancy of this scheme constitutes a key advantage, as two navigation solutions are available simultaneously: the standalone raw PPP solution and the integrated PPP/SADDCP solution. The loosely coupled architecture provides high flexibility and modularity, with reduced computational burden and complexity due to the independent processing of each subsystem. When at least five healthy satellites are available, E-PPP primarily relies on raw PPP because of its absolute positioning capability and high precision. When raw PPP becomes unavailable, due to cycle slips, severe multipath, or limited sky visibility, E-PPP relies on the Kalman-filter-smoothed SADDCP solution, provided that at least two satellites are available for a planar solution and three satellites for a full 3D solution. However, in completely GNSS-denied environments, E-PPP cannot continue operating, as both PPP and SADDCP are GNSS-dependent techniques.

2.2. Loosely Coupled Integration of SADDCP and MEMS-INS (R-NS)

The loosely coupled integration of SADDCP with a MEMS-based INS is also implemented using a self-developed MATLAB algorithm, resulting in the Relative Navigation System (R-NS). This integration combines the high relative accuracy and multipath resistance of SADDCP with the high-frequency and self-contained characteristics of the MEMS-INS. In this scheme, SADDCP is used to smooth and correct the noisy and unstable MEMS-INS observations through Kalman filtering. Conversely, the MEMS-INS assists in bridging short GNSS outages and mitigating the impact of cycle slips, allowing the integrated solution to maintain continuity during temporary signal interruptions. However, when GNSS signals become partially or completely unavailable, R-NS performance begins to degrade due to the inherent drift characteristics of the standalone MEMS-INS. The degradation rate increases with time in the absence of SADDCP updates. Another limitation of R-NS is its relative nature, since both SADDCP and MEMS-INS provide relative positioning information. Consequently, after long GNSS outages, the solution resumes from the last estimated position, which may significantly deviate from the true position. Despite these limitations, R-NS is suitable for many engineering applications requiring high-frequency and relatively precise measurements, such as distance determination, area and volume computation, deformation monitoring, and relative navigation tasks.

2.3. Uncoupled Integration of E-PPP and R-NS (EPPP-NS)

The third level of integration consists of an uncoupled integration between E-PPP and R-NS, producing the final Enhanced PPP Navigation System (EPPP-NS). In this framework, E-PPP serves as the primary reference solution whenever three or more GNSS satellites are available. When GNSS coverage becomes limited or temporarily unavailable, the E-PPP solution may degrade due to cycle slips and reduced satellite geometry. Under these conditions, EPPP-NS switches to the R-NS solution to maintain positioning continuity. Once GNSS coverage is restored, E-PPP is reactivated as the reference solution, and forward and reverse Kalman filtering are applied to mitigate the accumulated errors of R-NS during the outage period.

This integration strategy effectively addresses the main limitations of the individual techniques:

- The high satellite requirement and cycle slip sensitivity of raw PPP,
- The relative nature of SADDCP, and
- The noise and rapid drift characteristics of MEMS-based INS.

Simultaneously, EPPP-NS combines their strengths:

- The absolute positioning capability of PPP,
- The self-contained and high-frequency operation of MEMS-INS, and
- The high relative precision and reduced satellite requirement of SADDCP.

As a result, EPPP-NS provides a robust and adaptive navigation solution suitable for diverse GNSS environments, including open-sky, partially obstructed, high-multipath, and GNSS-denied scenarios.

The integration of raw PPP, SADDCP, and MEMS-based INS can be illustrated in the following flowchart:

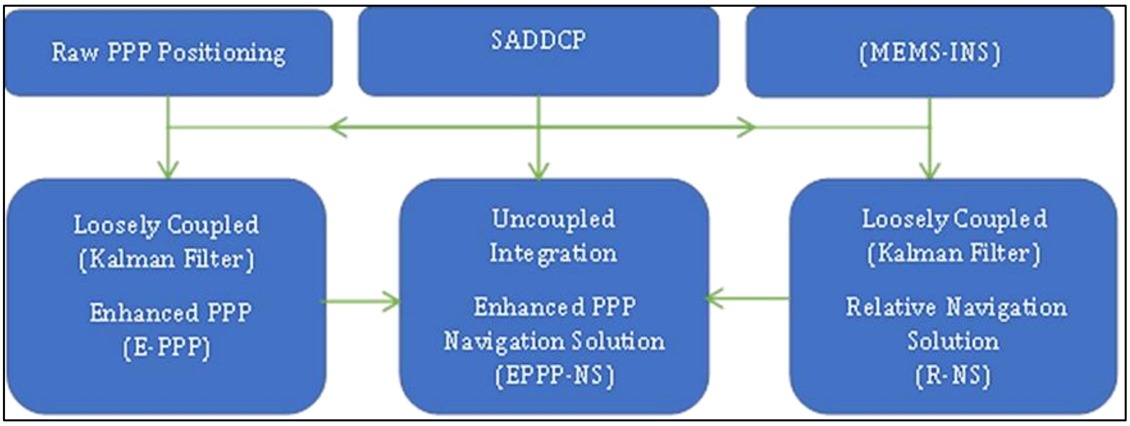

Figure 1 Flowchart of raw PPP/SADDCP/MEMS-based INS integration

3. Mathematical descriptions

3.1. Loosely Coupled Integration of SADDCP and PPP (E-PPP)

The GNSS carrier phase observable in meters can be written as:

$$CP\,(s,r)(k) = p\,(s,r)(k) + c\,(dT\,(s)(k) - dt\,(r)(k)) + dion\,(s,r)(k) + dtrop\,(s,r)(k) + dor\,(s)(k) + E\,(s,r)(k) + L * N$$

where,

- *CP (s,r)(k)* the carrier phase observation (m)
- *p (s,r)(k)* the true range between receiver *(r)* and satellite *(s)* at epoch *(k)*
- *c* the speed of light
- *dT (s)(k)* the clock error of satellite *(s)* at epoch *(k)*
- *dt (r)(k)* the clock error of receiver *(r)* at epoch *(k)*
- *dion (s,r)(k)* the ionospheric delay between receiver *(r)* and satellite *(s)* at epoch *(k)* (m)
- *dtrop (s,r)(k)* the tropospheric delay between receiver *(r)* and satellite *(s)* at epoch *(k)* (m)
- *dor (s)(k)* the orbit error of satellite *(s)* at epoch *(k)* (m)
- *E (s,r)(k)* the measurement noise between receiver *(r)* and satellite *(s)* at epoch *(k)*
- *L* the carrier wavelength (m)
- *N* the unknown integer ambiguity (cycle)

The true range between receiver *(r)* and satellite *(s)* at epoch *(k)* can be written as:

$$p\,(s,r)(k) = ((X(s) - X(r))2 + ((Y(s) - Y(r)) + ((Z(s) - Z(r)))0.5$$

where,

X, Y and *Z* the satellite and receiver Cartesian coordinates.

In SADDCP, the first single differencing is formed between one receiver (r), one satellite (s) and two adjacent epochs *((k)* and *(k + 1))*. The single differencing equation can be written as:

$$\begin{aligned} SD(s)(r)(k+1,k) &= CP(s,r)(k+1) - CP(s,r)(k) \\ &= [\,p(s,r)(k+1) + c(dT(s)(k+1) - dt(r)(k+1)\,) + dion(s,r)(k+1) + dtrop(s,r)(k+1) \\ &+ dor(s)(k+1) + E(s)(r)(k+1) + L\,N\,] - [\,p(s,r)(k) + c(dT(s)(k) - dt(r)(k)\,) \\ &+ dion(s,r)(k) + dtrop(s,r)(k) + dor(s)(k) + E(s)(r)(k) + L\,N\,] \end{aligned}$$

where,

$SD(s)(r)(k+1,k)$ *single differencing between receiver* (r)*, one satellite* (s) *and two adjacent epochs ((k) and (k + 1))*

From the single-differenced observations, the double-difference ambiguities are eliminated provided that the integer ambiguities remain constant and continuous satellite signal lock is maintained. The satellite clock error is significantly reduced due to the high stability of satellite clocks over short transmission intervals. Similarly, satellite orbit errors are largely mitigated because of their strong temporal correlation. The ionospheric and tropospheric errors are reduced to the change in delay over the considered time interval. Multipath effects, however, remain present, although they can be partially mitigated due to their temporal correlation characteristics. On the other hand, the receiver clock error is amplified (doubled), and the receiver measurement noise increases as a consequence of the differencing process. Accordingly, the final form of the single-difference observation equation can be expressed as:

$$SD(s)(r)(k+1,k) = p\,(s)(r)(k+1,k) - c\,dt\,(r)(k+1,k) + E\,(s)(r)(k+1,k)$$

The second differencing in SADDCP is carried out between two single differences, similar to that in equation (3), cross two satellites *(s)* and *(j)*. This can be written as:

$$\begin{aligned} DD(s,j)(r)(k+1,k) &= SD(s)(r)(k+1,k) - SD(j)(r)(k+1,k) \\ &= [\,p\,(s)(r)(k+1,k) - c\,dt\,(r)(k+1,k) + E\,(s)(r)\,(k+1,k)\,] - [\,p\,(j)(r)(k+1,k) \\ &- c\,dt\,(r)(k+1,k) + E\,(j)(r)(k+1,k)\,] \end{aligned}$$

where,

$DD(s,j)(r)(k+1,k)$ *double differences between one receiver (r), two epochs (k+1) and (k), and two satellites (s) and (j).*

The receiver clock error is completely eliminated in the double-difference observations. This is a crucial advantage for achieving high positioning accuracy, particularly when using low-cost receivers, whose oscillators are sensitive to temperature and pressure variations, resulting in unstable clock behavior. By forming double differences, both satellite and receiver clock errors are effectively cancelled, significantly enhancing the robustness of the carrier-phase measurements [25]. Accordingly, the final form of the double-difference observation equation can be expressed as:

$$DD(s,j)(r)(k+1,k) = p(s,j)(r)(k+1,k) + E(s,j)(r)(k+1,k)$$

The only unknown parameters in this equation are the receiver Cartesian coordinates at the two consecutive epochs, (k) and $(k+1)$. The change in receiver position between these two epochs can be determined by fixing the receiver coordinates at epoch (k) (for example, setting them to zero as a reference) and solving for the receiver coordinates at epoch $(k+1)$. Thus, the solution represents the relative displacement of the receiver between epochs (k) and $(k+1)$. To estimate the receiver's relative position at epoch $(k+1)$ with respect to epoch (k), the double-difference observation equation can be formulated as:

$$b = A\,X + v$$

where,

- b the measurement victor with a size of (number of epochs -1, 1)
- X the parameter victor with a size of (number of epochs * 3, 1) which include the change in Cartesian position across the interval
- A matrix with a size of (number of epoch -1, number of epoch * 3) relating parameters to states
- v a vector of random noise with a size of (number of epochs -1, 1)

This equation can then be solved by least squares as:

$$X = (A'\,w\,A) - 1\,A'\,w\,b$$

where,

w the weight matrix with a size of (number of epochs -1, number of epochs -1) which is based on the average satellite residuals obtained from the stand-alone code positioning calculations.

Kalman filter (KF) filters measurements based on the expected changes of these measurements over time and the statistical properties of the system measurement errors. The filter determines the minimum error estimate of the states based on the linear relation between the measurements and these states. The states are composed of number of values that adequate to define the system motion. KF consists of measurement model and dynamic model which will be illustrated here to define the basic elements as related to the integration of SADDCP with code positioning. As for the equations of propagation and update steps, they are well documented in different sources and there is no point for repeating here. The measurement model defines the mathematical linear relationship between the measurements and the filter states. The discrete measurement model at the epoch *(k)* can be defied as:

$$Z(k) = H\,U(k) + v(k)$$

where,

- *Z(k)* the vector of measurements at the epoch (k)
- *U(k)* the system state vector at the epoch (k)
- *H* the design matrix of the linear relationship between the states and the measurements
- *v(k)* the measurement residual vector

The dynamic model describes the change in the state vector parameters over time. The discrete dynamic Model between epochs *(k+1)* and *(k)* can be given as:

$$U(k+1) = M\,U(k) + W(k)$$

where,

- *M* *the state transition matrix of the relation between state vector parameters over time.*

- *W(k) the system noise is approximated based on the is the sampling interval, the spectral density matrix and standard deviations of the driving noise of the system.*

In the case of integrating PPP with SADDCP, the vector of measurements includes six observations; three observations from the raw PPP of epoch k $(X(K), Y(K), Z(K))$ and three values describing the 3D changes in positioning between epochs (k) and $(k+1)$ $(dX(K,K+1), dY(K,K+1), dZ(K,K+1))$. As there are no unknowns, the $Z(k)$ and $U(k)$ are the same vector, H is a (6*6) unit matrix and $v_{(k)}$ equal zero.

$$Z(k) = U(k) = |\, X(K)\; Y(K)\; Z(K)\; dX(K,K+1)\; dY(K,K+1)\; dZ(K,K+1)\, |'$$

$$H = \begin{bmatrix} 1 & 0 & 0 & 0 & 0 & 0 \\ 0 & 1 & 0 & 0 & 0 & 0 \\ 0 & 0 & 1 & 0 & 0 & 0 \\ 0 & 0 & 0 & 1 & 0 & 0 \\ 0 & 0 & 0 & 0 & 1 & 0 \\ 0 & 0 & 0 & 0 & 0 & 1 \end{bmatrix}$$

As for the dynamic model, the system state vector at the epoch *(k+1)* includes three observations from the absolute code positioning for this epoch (*X(K+1), Y(K+1), Z(K+1)*) and three values describing the 3D changes in positioning between this epoch and the previous one (*dX(K, K+1), dY(K, K+1), dZ(K, K+1)*). The system state vector can be defined as:

$$U(k+1) = |\, X(K+1)\; Y(K+1)\; Z(K+1)\; dX(K,K+1)\; dY(K,K+1)\; dZ(K,K+1)\, |'$$

The smoothed PPP positioning in epoch *(k+1)* can be defined as:

$$X(K+1) = X(K) + dX(K,K+1)$$
$$Y(K+1) = Y(K) + dY(K,K+1)$$
$$Z(K+1) = Z(K) + dZ(K,K+1)$$

To relate the state vectors in epoch *(k+1)* with that in epoch *(k),* the state transition matrix *(M)* should be written as:

$$M = \begin{bmatrix} 1 & 0 & 0 & 1 & 0 & 0 \\ 0 & 1 & 0 & 0 & 1 & 0 \\ 0 & 0 & 1 & 0 & 0 & 1 \\ 0 & 0 & 0 & 1 & 0 & 0 \\ 0 & 0 & 0 & 0 & 1 & 0 \\ 0 & 0 & 0 & 0 & 0 & 1 \end{bmatrix}$$

The standard deviations assigned to the SADDCP observations in the system noise vector $\mathrm{w}(k)$ of the dynamic model are computed using the signal-to-noise ratio (SNR) values obtained directly from the receiver RXM-RAW message. Since carrier-phase precision is strongly correlated with signal strength, the SNR provides a realistic and adaptive stochastic characterization of the phase measurements. Under multipath-free conditions, the standard deviation of carrier-phase observations is typically at the millimeter level. In degraded environments, it may increase and approach approximately one quarter of the GPS L1 wavelength (≈ 5 cm) [26], which can be considered a conservative upper bound. In this study, the discrepancy between the smoothed PPP position at epoch $(k+1)$ and the raw PPP solution at the same epoch is used as an indicator of PPP solution quality. This difference provides an adaptive assessment of the reliability of PPP observations at the subsequent epoch and can be used to adjust the stochastic model accordingly.

Since carrier-phase measurements are an essential component of the integration framework, cycle slip detection and correction are critical, particularly in urban environments where signal blockage and reconnection frequently occur. A cycle slip introduces an unknown integer number of cycles into the carrier-phase observation. In this work, cycle slips are detected using the geometry-free combination based on the difference between code and carrier-phase measurements across two consecutive epochs. Sudden discontinuities in this difference indicate the presence of a cycle slip. Code positioning provides a continuous solution as long as at least four satellites are available. Unlike carrier-phase positioning, code positioning does not require continuous tracking of the same satellites between epochs, as each epoch is independently solved. When a sufficient number of cycle-slip-free carrier-phase measurements is available, phase observations are used for precise relative positioning. Since receiver clock error is eliminated through the SADDCP double-differencing process, a minimum of three satellites is sufficient to estimate the 3D relative displacement. If fewer than three cycle-slip-free carrier-phase observations are available, pseudo-range measurements are used to bridge the gap and maintain solution continuity. However, when only three or fewer satellites are available, reliable quality assessment of the code solution becomes challenging due to insufficient redundancy. In such cases, integration with MEMS-INS becomes particularly beneficial. The inertial measurements provide short-term stability and can be assigned higher weights in the filter to maintain positioning robustness during GNSS degradation [13].

Satellite residuals are continuously monitored to detect and eliminate outliers using the Data Snooping method. The procedure starts with computing the covariance matrix of the observation residuals. Then, the standard deviation of each observation is extracted from the square roots of the diagonal elements and finally computing the standardized residual, which is expected to lie within the interval [0، 3], depending on the selected confidence level. For a 99% confidence level adopted in this study, the critical value is approximately 2.6. Any observation with residual bigger than 2.6 is classified as an outlier, with a 1% probability of incorrectly rejecting a valid observation (Type I error). Figure (2) illustrates the SADDCP filtering and cycle slip correction procedure, while Figure (3) presents the overall PPP/SADDCP integration framework.

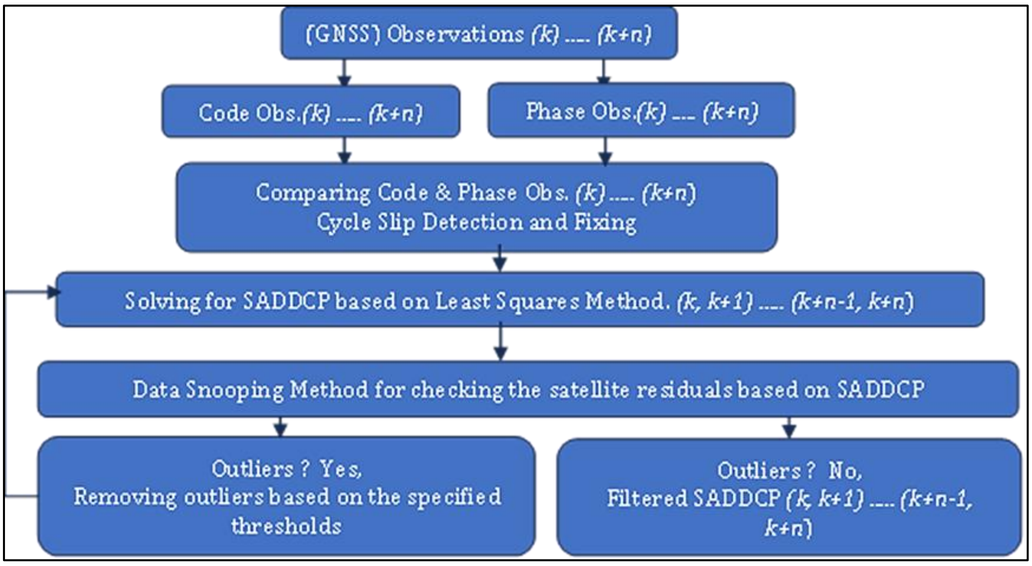

Figure 2 SADDCP: statistical testing, cycle slips detection and fixing

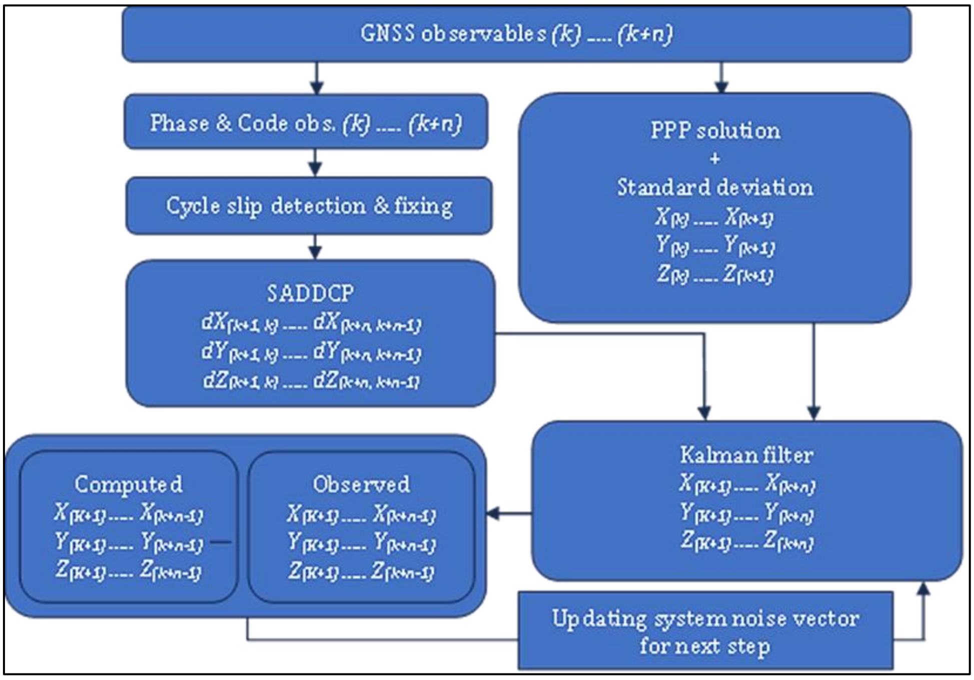

Figure 3 Workflow diagram of integrating SADDCP/PPP

3.2. Loosely Coupled Integration of SADDCP and MEMS-INS (R-NS)

Loosely Coupled (LC) integration is the typical integration of GNSS and INS. In this integration level, GNSS is run autonomously and, at the same time, GNSS/ INS integrated solution is enabled. The estimated position and velocity, provided by INS and GNSS, are compared and the differences are inputted to the estimation filter. The advantage of this approach comes from its redundancy where two navigation solutions are provided: that of GNSS and the other of GNSS/INS integration. This integration approach can be used with any INS and GNSS receiver if the necessary number of GNSS satellites is available. Also, loosely integration has high flexibility and modularity as well as less computation and complexity due to the independent operation. When GNSS is hidden or less than the necessary number of satellites are available, the INS stand-alone solution based on KF is used to fill in the gap, which will drift with time depending on the stability of the accelerometers and gyros used. In the case of integrating SADDCP/MEMS-INS, the vector of measurements includes six observations; three observations from the relative or absolute positioning of epoch (*k+1*):

$$(X\ SADDCP\ (K+1), Y\ SADDCP\ (K+1), Z\ SADDCP\ (K+1))$$

The three values describing the 3d changes in positioning between epochs *(k+1, k+2*) determined by MEMS-INS:

$$(\Delta X\ INS\ (K+1, K+2), \Delta Y\ INS\ (K+1, K+2), \Delta Z\ INS\ (K+1, K+2))$$

As there are no unknowns, the $Z_{(k)}$ and $U_{(k)}$ are the same vector, *H* is a (6*6) unit matrix, and $v_{(k)}$ equals zero as bellow:

$$Z(k+1) = U(k+1) = |X\ SADDCP\ (K+1)\ Y\ SADDCP\ (K+1)\ Z\ SADDCP(K+1)\ \Delta X\ INS\ (K+1, K+2)\ \Delta Y\ INS\ (K+1, K+2)\ \Delta Z\ INS\ (K+1, K+2)|'$$

$$H = \begin{bmatrix} 1 & 0 & 0 & 0 & 0 & 0 \\ 0 & 1 & 0 & 0 & 0 & 0 \\ 0 & 0 & 1 & 0 & 0 & 0 \\ 0 & 0 & 0 & 1 & 0 & 0 \\ 0 & 0 & 0 & 0 & 1 & 0 \\ 0 & 0 & 0 & 0 & 0 & 1 \end{bmatrix}$$

where,

- *Z(k)* the vector of measurements at epoch *(k)*
- *U(k)* the system state vector at epoch *(k)*
- *H* the design matrix of the linear relationship between the states and the measurements
- *v(k)* the measurement residual vector

As for the dynamic model, the system state vector at the epoch *(k+2)* includes three observations from SADDCP positioning for this epoch:

$$(X\ SADDCP\ (K+2), Y\ SADDCP\ (K+2), Z\ SADDCP\ (K+2))$$

And the three values describing the 3D changes in positioning between this epoch and the previous epoch and the system state vector can be defined as:

$$(\Delta X\ INS\ (K+1, K+2), \Delta Y\ INS\ (K+1, K+2), \Delta Z\ INS\ (K+1, K+2))$$

$$U(k+1) = |X\ SADDCP\ (K+2)\ Y\ SADDCP\ (K+2)\ Z\ SADDCP\ (K+2)\ \Delta X\ INS\ (K+1, K+2)\ \Delta Y\ INS\ (K+1, K+2)\ \Delta Z\ INS\ (K+1, K+2)|'$$

The smoothed integrated positioning in epoch *(k+2)* can be defined as:

$$X\ IP\ (K+2), Y\ IP\ (K+2), Z\ IP\ (K+2)$$
$$= X\ SADDCP\ (K+2), Y\ SADDCP\ (K+2), Z\ SADDCP\ (K+2)$$
$$+ \Delta X\ INS\ (K+1, K+2), \Delta Y\ INS\ (K+1, K+2), \Delta Z\ INS\ (K+1, K+2)$$

To relate the state vectors in epoch *(k+1)* with that in epoch *(k)*, the state transition matrix *(M)* takes the size of (6 *6) and can be written as:

$$M = \begin{bmatrix} 1 & 0 & 0 & 1 & 0 & 0 \\ 0 & 1 & 0 & 0 & 1 & 0 \\ 0 & 0 & 1 & 0 & 0 & 1 \\ 0 & 0 & 0 & 1 & 0 & 0 \\ 0 & 0 & 0 & 0 & 1 & 0 \\ 0 & 0 & 0 & 0 & 0 & 1 \end{bmatrix}$$

where,

- M the state transition matrix that defines the relation between state vector parameters over time.
- *W(k)* the system noise is approximated based on the sampling interval, the spectral density matrix and standard deviations of the driving noise of the system.

Because the SADDCP technique relies on temporal differencing between adjacent epochs, the resulting measurement quality depends on the correlation characteristics of multipath errors over time. If the reflected signal components exhibit high temporal correlation, differencing may partially cancel their effects, improving precision. Conversely, rapidly varying multipath can amplify the noise level after differencing. As a result, the navigation solution accuracy may remain at the millimeter level under favorable conditions but can degrade to nearly one decimeter in worst-case scenarios. This behavior contrasts with MEMS-INS measurements, whose precision is typically at the level of several decimeters due to sensor noise accumulation and bias instability. The loosely coupled (LC) integration of SADDCP with MEMS-INS is illustrated in the following workflow diagram, which has been implemented by the author in MATLAB.

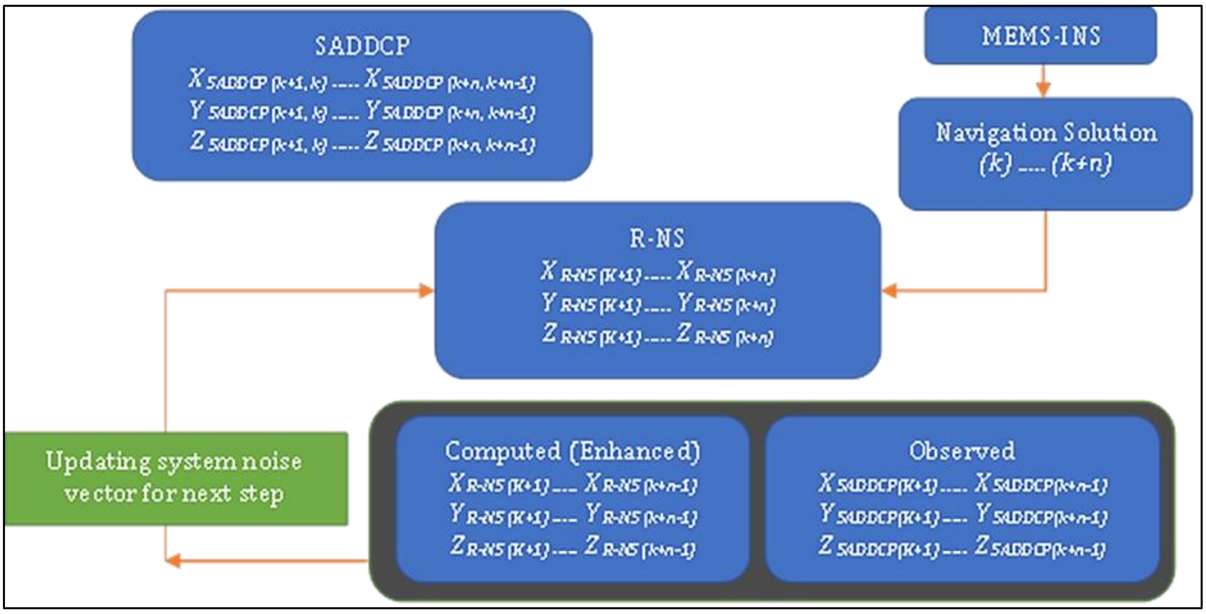

Figure 4 Workflow diagram of SADDCP/MEMS-INS integration

3.3. Uncoupled Integration of E-PPP and R-NS (EPPP-NS)

UC integration is the simplest level of integration as R-NS is reset at regular intervals of time using E-PPP, providing EPPP-NS, which can be obtained using the following formulas:

$$X\ EPPP - NS(k+2), Y\ EPPP - NS(k+2), Z\ EPPP - NS(k+2)$$
$$= X\ E - PPP(k+1), Y\ E - PPP(k+1), Z\ E - PPP(k+1) + \Delta X\ R - NS\ (k+1, k+2), \Delta Y\ R$$
$$- NS\ (k+1, k+2), \Delta Z\ R - NS\ (k+1, k+2)$$

where,

$$X\ EPPP-NS(k+2), Y\ EPPP-NS(k+2), Z\ EPPP-NS(k+2)$$

X, Y, Z coordinates of EPPP-NS at epoch *(k+2)*

$$X\ E-PPP(k+1), Y\ E-PPP(k+1), Z\ E-PPP(k+1)$$

X, Y, Z coordinates of E-PPP at epoch *(k+1)*

$$\Delta X\ R-NS\ (k+1, k+2), \Delta Y\ R-NS\ (k+1, k+2), \Delta Z\ R-NS\ (k+1, k+2)$$

R-NS between epoch *(k+1)* and *(k+2)*

4. Tests, results and discussion

The proposed system was experimentally evaluated in Benghazi, Libya. The selected vehicle trajectory was carefully designed to include a variety of GNSS operating conditions in order to assess system robustness under realistic environments. The test route was divided into four distinct segments, including: open-sky environment with healthy GNSS signal availability, weak GNSS environment under tree canopies, high-multipath environment between tall buildings, and GNSS outage segment, where the GNSS antenna was intentionally switched off. These four segments are illustrated in Figures (5) (6), (7), and (8), respectively with the performance of E-PPP, R-NS, and EPPP-NS. All collected datasets were post-processed using NovAtel Waypoint software to generate reference solution as well as raw PPP with quality values for each epoch, in addition to the self-developed MATLAB algorithms implementing the mathematical models described in the previous sections.

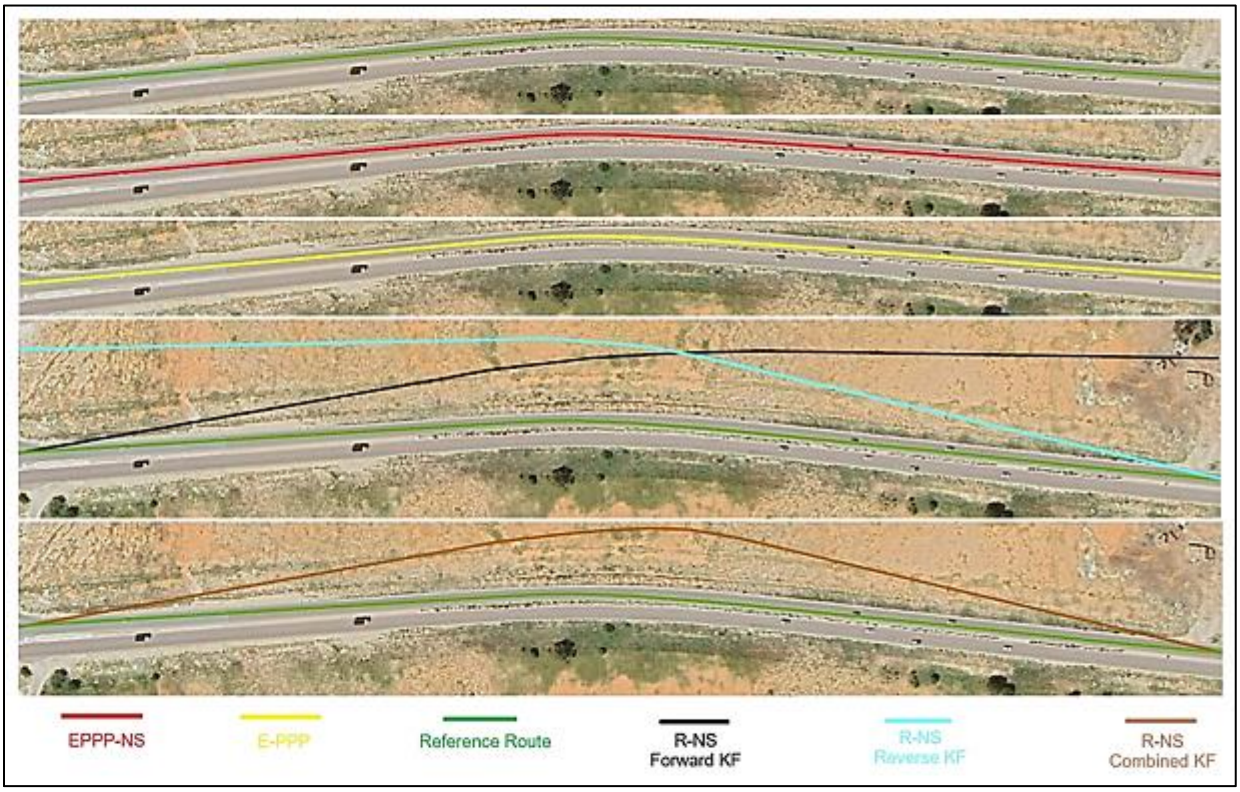

Figure 5 E-PPP, R-NS, and EPPP-NS, in GNSS open-sky

As clear from figure 5, in open sky, the performance of EPPP-NS is identical with E-PPP and nearly matches the reference route with Root Mean Square Error (RMSE) of about 2cm in E and N components, and 3 cm in H component. This can be referred to the fact that in open-sky with significant number of healthy satellites, EPPP-NS depends completely on E-PPP where the weights of E-PPP solution will be considerable compared to MEMS-based INS. R-NS has shown a smooth and comparable performance in open-sky areas, especially when applying two-way KF, but it drifts with time by nearly

2.8 mm/s and needs a number of absolute points along the trajectory for projecting the relative solution and banding the drifts. This is expected as R-NS is based on two relative positioning and navigation techniques, and thus, the errors are cumulative.

When GNSS signals became weak due to trees, as shown in figure (6), the performance of E-PPP has degraded compared to open-sky areas with RMSE values fluctuates from a few centimeters to a few decimeters, which can be as a result of reducing the number of satellites and bad dilation of precision (DOP). However, E-PPP has provided continues solution without interruption as E-PPP can benefit from the ability of SADDCP to continually work even with 2 connected satellites, which is not the case with PPP solution as at least 5 healthy satellites should be available. R-NS has also provided continues solution in weak GNSS areas benefits from the high ability of SADDCP to work with limited number of satellites and the INS measurements that are smoothed by KF. EPPP-NS has shown an excellent performance with RMSE of a few centimeters, gathering the advantages of both: E-PPP and R-NS. EPPP-NS has provided an absolute, continues, and precise solution, where PPP provides absolute and precise solution before and after weak GNSS areas, SADDCP helps when the number of satellites is limited, INS measurements fill in the gaps of both PPP and SADDCP when GNSS is weak and solving the detected cycle slips, and KF smoothing the measurements in forward and reverse directions based on good prediction values.

Figure 6 E-PPP, R-NS, and EPPP-NS, in weak GNSS area

Between buildings, the effect of multipath becomes sizable which can be noted from the satellite residuals, however, as long as 5 healthy satellites are available with small residuals, EPPP-NS and E-PPP show identical and normal performance. When the number of satellites reduces to 3, EPPP-NS and E-PPP provides continues solutions, but with higher quality for EPPP-NS, which can be referred to the advantage of using INS measurements to facilitate as well as accelerate fixing cycle slips and as consequence, increasing the number of satellites as well as improving the quality of satellite geometry. However, in some parts of "between buildings areas" as clear from figure (7), E-PPP solution has been completely lost and EPPP-NS has shown a relatively degraded performance though the number of detected satellites is sufficient, which can be referred to the high effect of multipath that can affect the correlation processing between the received satellite code and the receiver generated code leading to losing the communication between the satellite and receiver. In such case, EPPP-NS can benefit from the smoothed INS measurements for providing continues solution but the quality depends on the period after which the full E-PPP solution will be updated by new PPP position, where the longer the updating period the more drifting from the right trajectory can be detected.

Between buildings, the effect of multipath becomes sizable which can be noted from the satellite residuals, however, as long as 5 healthy satellites are available with small residuals, EPPP-NS and E-PPP show identical and normal performance. When the number of satellites reduces to 3, EPPP-NS and E-PPP provides continues solutions, but with higher quality for EPPP-NS, which can be referred to the advantage of using INS measurements to facilitate as well as accelerate fixing cycle slips and as consequence, increasing the number of satellites as well as improving the quality of satellite geometry. However, in some parts of "between buildings areas" as clear from figure (7), E-PPP solution has been completely lost and EPPP-NS has shown a relatively degraded performance though the number of detected satellites is sufficient, which can be referred to the high effect of multipath that can affect the correlation processing between the received satellite code and the receiver generated code leading to losing the communication between the satellite and receiver. In such case, EPPP-NS can benefit from the smoothed INS measurements for providing continues solution but the quality depends on the period after which the full E-PPP solution will be updated by new PPP position, where the longer the updating period the more drifting from the right trajectory can be detected.

Figure 7 E-PPP and EPPP-NS, in high multipath area

Last figure shows the performance of the integrated solutions when GNSS signals are hidden. GNSS antenna has been switched off to simulate passage through tunnels, under large bridges, and into very dense forests. E-PPP as well as R-

NS have failed to provide any solution due to the main dependency on GNSS signals. EPPP-NS has shown acceptable performance at the beginning and the end of the trajectory for a period, where the influence of the previous healthy PPP, SADDCP on MEMS-based INS measurements via Kalman filter is still effective. However, the performance of EPPP-NS degrades with time before deteriorating further at the first turn of the road. Since the role of PPP and SADDCP have been disabled due to the interruption of GNSS-receiver communications, EPPP-NS starts depending on the smoothed R-NS, and as SADDCP is off, R-NS will depend on smoothed INS measurements. As a consequence, EPPP-NS depends on INS when GNSS is off. Weights that are used for INS measurements in KF plays a significant roles in the performance of R-NS and as a result, using high weights for INS observations leads to fast deteriorations in the navigation solution as each small vibration will be translated to big displacements in positioning, especially in heading direction where vertical gravity correction do not have any ability to band the drifts. The opposite is also not recommended, where providing INS observations with low-weights guides to neglect the actual sensitivity of IMU gyros and accelerometers, providing distorted path on both displacements and directions.

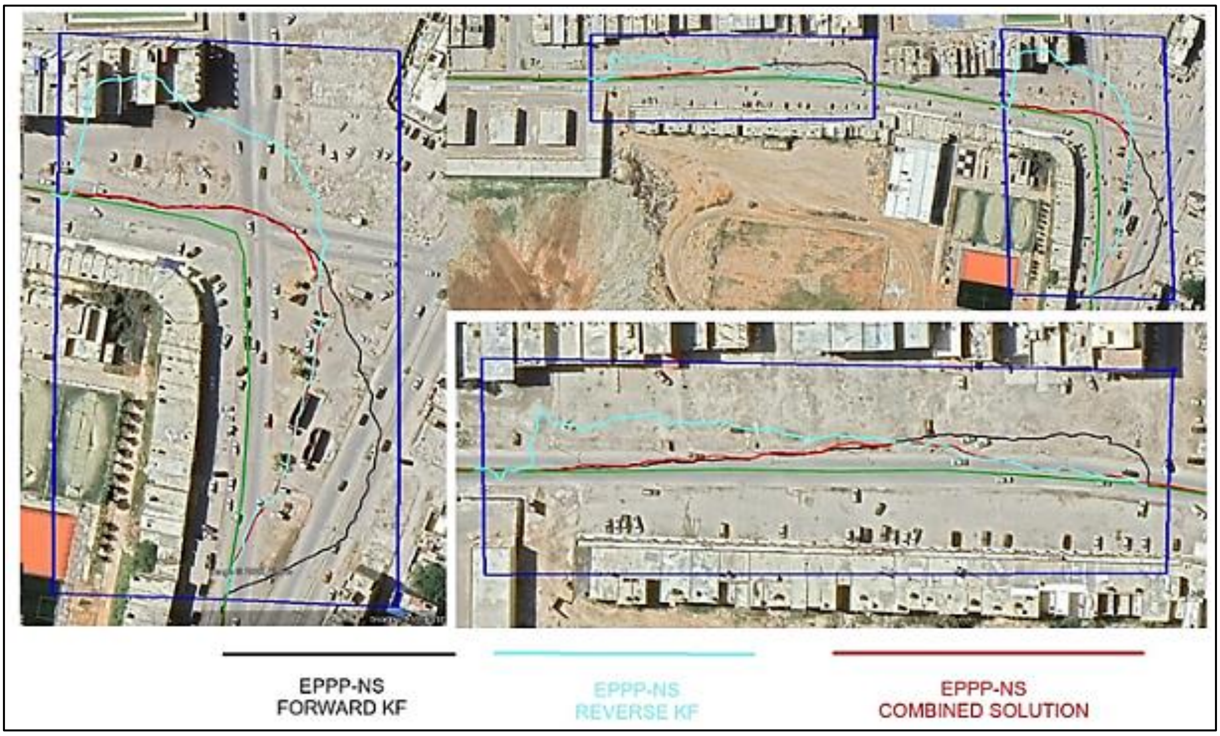

Figure 8 EPPP-NS, when GNSS is off

5. Conclusion and recommendations

This study presented the development and experimental validation of an Enhanced PPP Navigation Solution (EPPP-NS), achieved through the integration of Precise Point Positioning (PPP), Stand-Alone Double-Differenced Carrier Phase (SADDCP), and MEMS-based Inertial Navigation Systems (MEMS-INS). The proposed framework was designed to exploit the complementary strengths of absolute positioning (PPP), relative carrier-phase positioning (SADDCP), and short-term inertial stability (MEMS-INS), while mitigating their individual limitations. The EPPP-NS architecture was implemented through three integration stages: (1) a loosely coupled PPP/SADDCP integration to produce the Enhanced PPP (E-PPP) solution, (2) a loosely coupled SADDCP/MEMS-INS integration to generate the Relative Navigation Solution (R-NS), and (3) an uncoupled fusion of E-PPP and R-NS to obtain the final EPPP-NS output. The system was evaluated using a pre-surveyed reference trajectory under four representative GNSS environments: open-sky conditions, weak GNSS availability, high-multipath urban scenarios, and complete GNSS outages.

Experimental results demonstrate that, under open-sky conditions, E-PPP achieves positioning accuracy comparable to raw PPP, with minor improvements observed in the vertical component due to carrier-phase smoothing. In partially obstructed environments, E-PPP enhances solution continuity and improves positioning robustness relative to conventional PPP. However, in severely degraded GNSS conditions, particularly under high multipath or insufficient satellite visibility, E-PPP performance deteriorates and ultimately becomes unavailable when the number of tracked satellites drops below the minimum required for planar or full 3D positioning. The R-NS solution, while inherently relative and requiring initialization from a known reference point, provides smooth short-term navigation performance. Under open-sky conditions, it maintains acceptable accuracy over limited durations before accumulating time-dependent drift due to the absence of absolute error bounding. In obstructed environments, R-NS effectively mitigates cycle slips in SADDCP by leveraging smoothed INS observations and ensures solution continuity. Nevertheless, drift remains the dominant error source over extended intervals.

Among the evaluated approaches, EPPP-NS consistently delivered the most stable, continuous, and robust navigation solution across all tested scenarios. In open-sky conditions, its performance matches that of E-PPP. In partially obstructed environments, short interruptions in the E-PPP solution are effectively bridged using the inertial-supported R-NS output, resulting in continuous and smooth positioning. In high-multipath areas, EPPP-NS maintains reliable and precise navigation as long as satellite tracking is preserved. When GNSS signals are temporarily lost, the solution exhibits gradual inertial drift until satellite availability is restored. The combined Kalman filtering strategy significantly reduces positioning errors in both horizontal and vertical components. During complete GNSS outages, EPPP-NS maintains acceptable short-term performance due to the influence of previously validated SADDCP updates propagated through the Kalman filter. However, beyond this interval, accuracy degrades progressively as inertial errors accumulate, with performance strongly dependent on IMU quality, vehicle dynamics, and stochastic weighting strategy.

Overall, the results confirm that the proposed EPPP-NS framework substantially enhances robustness, continuity, and stability compared to E-PPP or relative SADDCP/INS integration. The method is therefore well-suited for engineering applications requiring reliable positioning in challenging GNSS environments, including UAV surveying in urban areas, mobile mapping, GIS data acquisition, and urban vehicle navigation under limited satellite visibility and severe multipath conditions.

Compliance with ethical standards

Acknowledgments

I would like to express my special thanks to my wife "Eng. Nagla Fadeil"

References

[1] Hofmann-Wellenhof B, Lichtenegger H, Wasle E. GNSS global navigation satellite systems: GPS, GLONASS, Galileo, and More. 2007

[2] Amami M, Smith M, Kokkas N. Low-Cost Vision Based Personal Mobile Mapping System. ISPRS- International Archives of The Photogrammetry, Remote Sensing and Spatial Information Sciences. 2014; XL-3/W1: 1-6.

[3] Amami M. Investigations into the quality of final-product dual frequency kinematic PPP in open sky using CSRS-PPP free online service: GPS Vs. GPS+GLONASS. Global Journal of Engineering and Technology Advances (GJETA). November 2025; 25(2):138-143.

[4] Amami M. Investigations into the quality of final-product dual-frequency static PPP over fixing time using CSRS-PPP free online service: GPS Vs. GPS + GLONASS. World Journal of Advanced Engineering Technology and Sciences (GJETA). November 2025; 17(2): 438-443.

[5] Amami M. Kinematic PPP Using PPP-WIZARD Free Online Service: GPS Vs. GPS + GLONASS. International Research Journal of Modernization in Engineering Technology and Science. December 2025; 7(12): 3445-3451.

[6] Amami M. A Novel Design Concept of Cost-Effective Permanent Rail-Track Monitoring System. World Journal of Advanced Research and Reviews. March 2022; 13(3): 451-473.

[7] Amami M, Fadeil A. Investigations into the quality of Kinematic PPP in open-sky using final-product APPS free online GPS-alone service. GSC Advanced Research and Reviews. January 2026; 26(1): 023:028

[8] Amami M. Quality of Static PPP over observation time using PPP-WIZARD free online service: GPS Vs. GPS + GLONASS. Open Access Research Journal of Science and Technology. December 2025; 15(2): 195-200

[9] Amami M, EL-Turki A, Rustum A, EL-Amaari I, Jabir T. Topographic Surveying using low-cost amateur drones and 4K ultra-high-definition videos. Open Access Research Journal of Science and Technology. April 2022; 4(2): 072-082.

[10] Amami M, Elmehdwi A, Borgaa A, Buker A, Alareibi A. Investigations into utilizing low-cost amateur drones for creating ortho-mosaic and digital elevation model. International research journal of modernization in engineering technology and science. March 2022; 4(3): 2107-2118.

[11] Amami M. Dual-Frequency Static PPP Over Fixing Time Using Final-Product Free Online Services: CSRS-PPP Vs. PPP-WIZARD Vs. APPS. Global Journal of Engineering and Technology Advances. February 2026; 26(02): 039-047

[12] Amami M. Dual-Frequency Kinematic PPP in Free-Multipath Open-Sky: CSRS-PPP vs. PPP-WIZARD Vs. APPS. International Journal for Research in Applied Science and Engineering Technology. February 2026; 14(I): 1005-1014.

[13] Amami M. The Integration of Stand-Alone GPS Code Positioning, Carrier Phase Delta Positioning and MEMS-Based INS. International Research Journal of Modernization in Engineering Technology and Science. March 2022; 4(3): 700-715.

[14] Amami M. The Integration of Time-Based Single Frequency Double Differencing Carrier Phase GPS/ Micro-Elctromechanical System-Based INS. International Journal of Recent Advances in Science and Technology. Dec. 2018; 5(4): 43-56.

[15] Amami M. The Integration of Image-Based Navigation and GPS Carrier Phase Delta Positioning for Aerial Triangulation using Low-Cost Drones with Limited Number of Ground Control Points. Quest Journals. 2022; 7(5): 23-31.

[16] Amami M. Enhancing Stand-Alone GPS Code Positioning Using Stand-Alone Double Differencing Carrier Phase Relative Positioning. Journal of Duhok University (Pure and Eng. Sciences). 2017; 20(1): 347 355.

[17] Amami M. Enhancing the Quality of Kinematic PPP in Partially and Heavily Obscured-Sky Using Stand-Alone Double Differencing Carrier Phase Relative Positioning. Open Access Research Journal of Science and Technology. February 2026; 16(01): 065-076.

[18] Amami M. The Advantages and Limitations of Low-Cost Single Frequency GPS/MEMS-Based INS Integration. Global Journal of Engineering and Technology Advances. Feb. 2022; 10(2): 018-031.

[19] Amami M. Comparison Between Multi and Single Epipolar Geometry-Based Filters for Optical Robot Navigation. International Research Journal of Modernization in Engineering Technology and Science. March 2022; 4 (3): 476-485.

[20] Amami M. Fast and Reliable Vision-Based Navigation for Real Time Kinematic Applications. International Journal for Research in Applied Sciences and Engineering Technology. Feb. 2022; 10(2): 922-932.

[21] Amami M. Comparison Between Multi Epipolar Geometry and Conformal 2D Transformation-Based Filters for Optical Robot Navigation. International Journal for Research in Applied Sciences and Engineering Technology. March 2022; 10(3): 388-398.

[22] Amami M. Comparison Between Multi Epipolar Geometry and Affine 2D Transformation-Based Filters for Optical Robot Navigation. International Journal for Research in Applied Sciences and Engineering Technology. March 2022; 10(3): 399-409.

[23] Amami M. Speeding up SIFT, PCA-SIFT and SURF Using Image Pyramid. Journal of Duhok University, [S.I]. July 2017; 20(1): 356-362.

[24] Amami M. Multi and Single Epipolar Geometry-Based Filters Vs. Affine and conformal 2D Transformation-Based Filters. Global Journal of Engineering and Technology Advances. March 2022; 10(3): 032-051.

[25] Amami M. Testing Patch, Helix and Vertical Dipole GPS Antennas with/without Choke Ring Frame. International Journal for Research in Applied Sciences and Engineering Technology. Feb. 2022; 10(2): 933-938.

[26] Amami M, Fadeil A. Evaluating The Quality Of Static PPP Over Observation Time Using APPS Free Online GPS-Alone Service. International Journal of Engineering Development and Research. January 2026; 14(1): 787-792